Mutant Mice Lacking the p53 C-Terminal Domain Model Telomere Syndromes

Iva Simeonova, Sara Jaber, Irena Draskovic, Boris Bardot, Ming Fang, Rachida Bouarich-Bourimi, Vincent Lejour, Laure Charbonnier, Claire Soudais, Jean-Christophe Bourdon, et al.

Cell Reports
Article

Mutant Mice Lacking the p53 C-Terminal Domain Model Telomere Syndromes

Iva Simeonova,[1,5,6] Sara Jaber,[1,5,6,9] Irena Draskovic,[2,5,6,9] Boris Bardot,[1,5,6] Ming Fang,[1,5,6] Rachida Bouarich-Bourimi,[1,5,6] Vincent Lejour,[1,5,6] Laure Charbonnier,[1,5,6] Claire Soudais,[3,7] Jean-Christophe Bourdon,[8] Michel Huerre,[4] Arturo Londono-Vallejo,[2,5,6] and Franck Toledo[1,5,6,*]

[1]Genetics of Tumor Suppression
[2]Telomeres and Cancer "Équipe Labellisée Ligue"
[3]CD4+T-Lymphocytes and Anti-Tumour Response
[4]Pathology Service
Institut Curie, Centre de Recherche, 26 rue d'Ulm, 75248 Paris Cedex 05, France
[5]UPMC Paris 06, 26 rue d'Ulm, 75248 Paris Cedex 05, France
[6]CNRS UMR 3244, 26 rue d'Ulm, 75248 Paris Cedex 05, France
[7]INSERM U932, 26 rue d'Ulm, 75248 Paris Cedex 05, France
[8]Ninewells Hospital, University of Dundee, Dundee DD19SY, Scotland
[9]These authors contributed equally to this work
*Correspondence: franck.toledo@curie.fr
http://dx.doi.org/10.1016/j.celrep.2013.05.028

SUMMARY

Mutations in p53, although frequent in human cancers, have not been implicated in telomere-related syndromes. Here, we show that homozygous mutant mice expressing $p53^{\Delta 31}$, a p53 lacking the C-terminal domain, exhibit increased p53 activity and suffer from aplastic anemia and pulmonary fibrosis, hallmarks of syndromes caused by short telomeres. Indeed, $p53^{\Delta 31/\Delta 31}$ mice had short telomeres and other phenotypic traits associated with the telomere disease dyskeratosis congenita and its severe variant the Hoyeraal-Hreidarsson syndrome. Heterozygous $p53^{+/\Delta 31}$ mice were only mildly affected, but decreased levels of Mdm4, a negative regulator of p53, led to a dramatic aggravation of their symptoms. Importantly, several genes involved in telomere metabolism were downregulated in $p53^{\Delta 31/\Delta 31}$ cells, including *Dyskerin*, *Rtel1*, and *Tinf2*, which are mutated in dyskeratosis congenita, and *Terf1,* which is implicated in aplastic anemia. Together, these data reveal that a truncating mutation can activate p53 and that p53 plays a major role in the regulation of telomere metabolism.

INTRODUCTION

Mutations in *TP53*, the gene encoding transcription factor p53, are frequently observed in sporadic cancers (Nigro et al., 1989), and germline *TP53* mutations cause the Li-Fraumeni syndrome of cancer predisposition (Malkin et al., 1990; Srivastava et al., 1990). These and other findings established p53 as a major tumor suppressor (Lane and Levine, 2010). In recent years, however, p53 emerged as a protein with a wide variety of functions: it is now thought to regulate longevity, fertility, and the production of stem cells and is involved in diseases including diabetes and several neurological disorders (Brady and Attardi, 2010).

Most p53 mutations in cancers affect the core DNA-binding domain of the protein, altering its capacity to regulate transcriptional target genes (Toledo and Wahl, 2006). Importantly, however, p53 contains a second DNA-binding domain in its carboxyl terminus (Foord et al., 1991), whose role remains elusive (Hupp et al., 1992; McKinney et al., 2004). Early studies suggested that the p53 C-terminal domain (CTD), whose interaction with DNA is not sequence dependent, acts as a negative regulator of the core DNA-binding domain (Hupp et al., 1992). However, later reports concluded that p53 requires its CTD for efficient recognition of target gene sequences (McKinney et al., 2004; Tafvizi et al., 2011; Hamard et al., 2012; Kim et al., 2012). The phosphorylation of C-terminal serines 378 and 392 was proposed to increase p53 DNA binding (Hupp et al., 1992; Takenaka et al., 1995), but only the latter was mutated and analyzed in vivo (Bruins et al., 2004). Furthermore, posttranslational modifications of C-terminal lysines were proposed to be essential for the regulation of p53 stability and activity, but mice with C-terminal lysines mutated into arginines appeared similar to wild-type (WT) mice (Feng et al., 2005; Krummel et al., 2005), except for a hypersensitivity to γ-irradiation (Wang et al., 2011a). Importantly, in vitro data suggested that a deletion of the p53 CTD, or mutations of C-terminal lysines, might cause distinct phenotypes because the CTD is required for an optimal interaction of p53 with Mdm2, a ubiquitin ligase that regulates p53 stability (Poyurovsky et al., 2010).

Here, we targeted a nonsense mutation at the mouse *Trp53* locus to evaluate the consequences of a deletion of the p53 CTD in vivo. The results we obtained clearly demonstrate that a deletion of the CTD leads to increased p53 activity. Most mice expressing a p53 lacking the CTD died rapidly after birth and exhibited features typical of telomere syndromes, including aplastic anemia, lung fibrosis, and short telomeres. Consistent with these observations, we found that p53 activation leads to the downregulation of several genes involved in telomere

metabolism including *Dyskerin*, a gene frequently mutated in dyskeratosis congenita (DC), the archetypal telomere syndrome (Armanios and Blackburn, 2012). These data provide evidence that p53 plays an important role in the regulation of telomere metabolism.

RESULTS

Rationale for the Targeting of a Nonsense Mutation Affecting the p53 CTD

In most in vitro studies, p53 mutants lacking the last 30–33 residues were analyzed. These mutants lacked a region enriched in basic residues (lysines, arginines, and histidines within residues 363–382 in human p53) and most if not all the C-terminal residues subject to posttranslational modifications (lysines, serines, and threonines within residues 362–392 in human p53). However, they retained an intact tetramerization domain (within residues 326–355 in human p53) (Figure S1A). Here, we aimed to analyze the consequences of a similar deletion of the p53 CTD in vivo and, thus, to target a nonsense mutation leading to a mouse p53 mutant that lacks the last 30–33 residues.

However, targeting a nonsense mutation at the murine *Trp53* locus presented two possible obstacles. First, a mutation removing the last 30–33 residues, within the penultimate exon (exon 10), might cause nonsense-mediated mRNA decay. Second, *Trp53* encodes, from mutually exclusive final exons, isoforms with two distinct CTDs: exon 11, used predominantly, encodes the "classical" p53 protein, whereas exon AS (for alternative splicing) encodes mouse-specific isoforms with a shorter C terminus (Arai et al., 1986). Therefore, although a mutation in exon 11 encoding a protein with a deletion of at most 26 residues would prevent mRNA degradation, we were concerned that it might perturb mRNA splicing and lead to compensatory p53AS overexpression (Figure S1B). These possibilities prompted us to perform preliminary experiments in which constructs encoding proteins with deletions of the last 26 ($p53^{\Delta 26}$) or 31 ($p53^{\Delta 31}$) residues were targeted in mouse embryonic fibroblasts (MEFs) by recombinase-mediated cassette exchange (RMCE) (Figures S1C and S1D). Neither mutation led to measurable decreases in p53 activity or p53 mRNA levels, but the mutation encoding $p53^{\Delta 26}$ was associated with a 9-fold increase in p53AS mRNAs (Figures S1E–S1J). From these data, we decided to create a mouse with a nonsense mutation deleting the last 31 residues.

$p53^{\Delta 31/\Delta 31}$ MEFs Exhibit Increased p53 Activity

To generate a mouse expressing $p53^{\Delta 31}$ conditionally, we used a targeting vector containing the mutation in exon 10 and transcriptional Stops flanked by LoxP sites (LSL) upstream of coding sequences (Figures 1A–1D). F1 intercrosses then produced $p53^{LSL\text{-}\Delta 31/LSL\text{-}\Delta 31}$ MEFs (Figure 1E). To analyze the effect of the targeted mutation, we first excised the LSL cassette ex vivo by adding Cre recombinase to $p53^{LSL\text{-}\Delta 31/LSL\text{-}\Delta 31}$ MEFs or to $p53^{LSL\text{-}WT/LSL\text{-}WT}$ MEFs (Ventura et al., 2007) as controls (Figures 2A and 2B). Similar p53 mRNA levels were found in the resulting $p53^{WT/WT}$ and $p53^{\Delta 31/\Delta 31}$ MEFs, but mutant cells contained higher mRNA levels of the p53 targets *p21*(*Cdkn1a*) and *Mdm2*, indicating an increased p53 activity (Figures 2C and 2D).

$p53^{+/LSL\text{-}\Delta 31}$ mice were also mated with PGK-Cre mice to obtain MEFs expressing $p53^{\Delta 31}$ constitutively, analyzed below. Immunofluorescence revealed that the $p53^{\Delta 31}$ protein is mostly nuclear, more abundant than $p53^{WT}$, and that it accumulates in response to stress (Figure 2E). Western blots confirmed the increased p53 levels in mutant cells (Figure 2F). $p53^{\Delta 31}$ protein levels were regulated by the ubiquitin ligase Mdm2, as indicated by treatment with Nutlin, a specific Mdm2 inhibitor (Figure 2G). The p21 and Mdm2 protein levels were increased in $p53^{\Delta 31/\Delta 31}$ MEFs (Figure 2F), and both genes were transactivated more efficiently in mutant cells (Figure 2H), although $p53^{\Delta 31}$ did not appear to bind specific sequences at the *p21* and *Mdm2* promoters more efficiently than $p53^{WT}$ (Figure 2I). Additional experiments confirmed that p53 target genes are more efficiently regulated in $p53^{\Delta 31/\Delta 31}$ cells (Figure S2A). Mutant MEFs presented increased G1/S ratios before or after irradiation (Figures 2J and S2B) and ceased to proliferate prematurely (Figures 2K and 2L). Together, these data demonstrated that $p53^{\Delta 31/\Delta 31}$ cells exhibit increased p53 activity.

$p53^{\Delta 31/\Delta 31}$ Mice Model Telomere Syndromes

$p53^{\Delta 31/\Delta 31}$ mice were born in Mendelian proportions from $p53^{+/\Delta 31}$ intercrosses, but most died 14–43 days after birth (Figure 3A). Because a mutation removing the last 31 residues of the CTD prevents the expression of isoforms with an AS C terminus (Figure S1B), we also generated mice with a specific deletion of exon AS. None of these mutants died within 3 months after birth (Figure S3), indicating that the premature death of $p53^{\Delta 31/\Delta 31}$ mice does not result from a loss of p53AS isoforms. The $p53^{\Delta 31/\Delta 31}$ mice that died within a month were significantly smaller than their littermates (Figure 3B), as reported for mice with an increased p53 activity (Mendrysa et al., 2003; Liu et al., 2007, 2010). Other evidence of increased p53 activity (Liu et al., 2007; Terzian et al., 2007; McGowan et al., 2008) in $p53^{\Delta 31/\Delta 31}$ mice included darker footpads and tails (Figures 3C and S4A), increased thymocyte apoptosis (Figures 3D and S4B), cerebellar hypoplasia, and hypogonadism in males (Figures S4C and S4D). $p53^{\Delta 31/\Delta 31}$ mice suffered from severe pancytopenia and had hypertrophic hearts typical of anemic animals (Figures 3E and 3F). A dramatic decrease in marrow cellularity was observed in $p53^{\Delta 31/\Delta 31}$ mice (Figure 3G), and mutant bone marrow cells (BMCs) lacked hematopoietic progenitors (Figures 3H, 3I, S4E, and S4F). Thus, the premature death of most $p53^{\Delta 31/\Delta 31}$ animals likely results from aplastic anemia and consecutive heart failure, consistent with previous reports of hematopoietic defects correlating with spontaneous perinatal death (Liu et al., 2007, 2010), accelerated aging (Dumble et al., 2007), or increased radiosensitivity (Mendrysa et al., 2003; Herrera-Merchan et al., 2010; Wang et al., 2011a) in mouse models with increased p53 activity.

Strikingly, $p53^{\Delta 31/\Delta 31}$ mice also developed pulmonary fibrosis (Figures 4A and 4B). In humans, the association of aplastic anemia and pulmonary fibrosis characterizes syndromes caused by abnormally short telomeres (Parry et al., 2011b). We compared the length of telomeres in WT and $p53^{\Delta 31/\Delta 31}$ cells and found shorter telomeres in mutant cells (Figures 4C and 4D). Furthermore, telomere dysfunction-induced foci were more frequent in $p53^{\Delta 31/\Delta 31}$ cells (Figure S5). This led us to conclude that

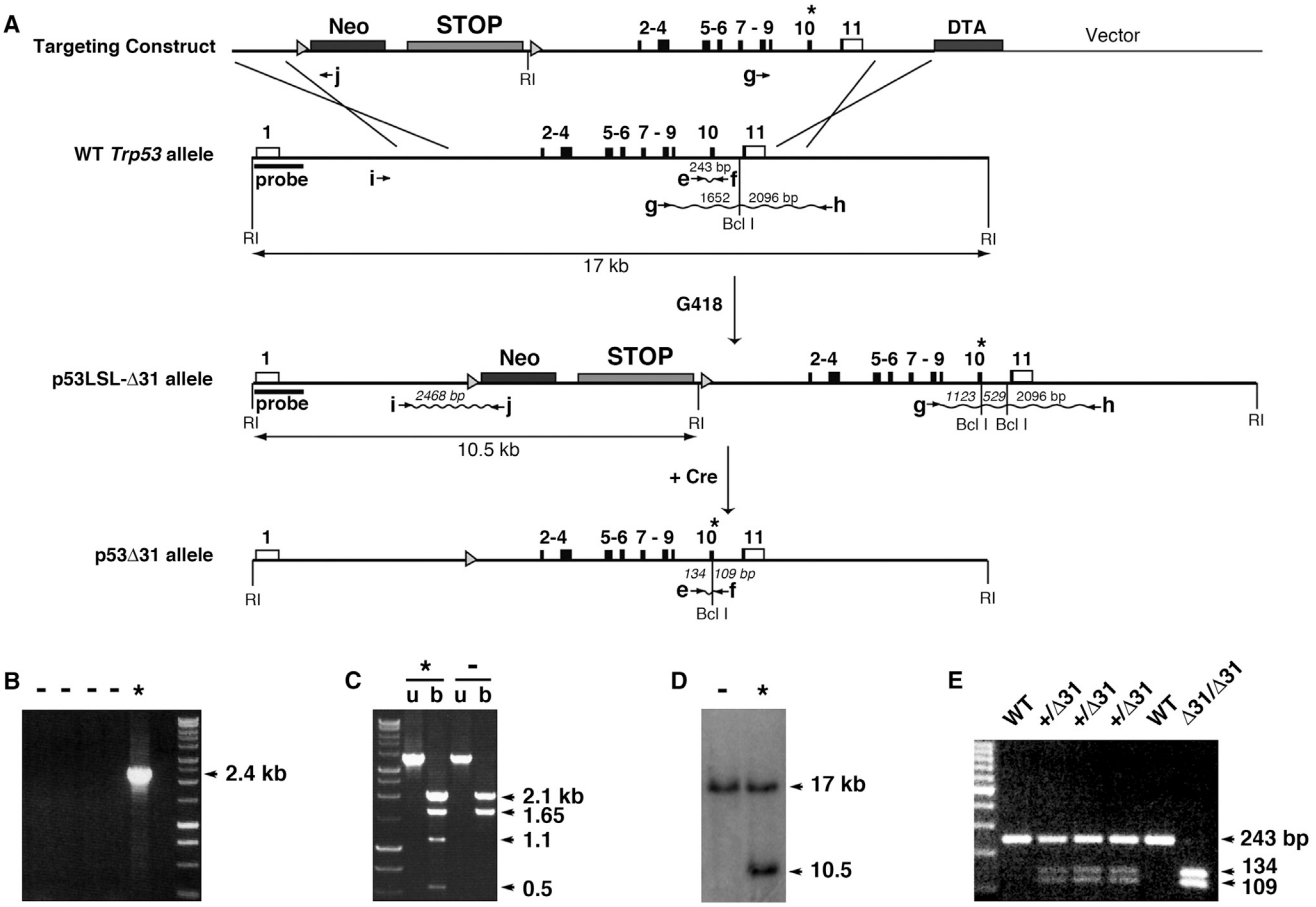

Figure 1. Targeting a Deletion of the CTD at the Mouse *Trp53* Locus

(A) Targeting strategy. The *Trp53* gene is within a 17-kb-long EcoRI (RI) fragment (black boxes indicate coding sequences; white boxes show UTRs). The targeting construct (above) contains (1) a 1.5-kb-long 5′ homology region; (2) a LSL cassette with a *neomycin* selection gene (Neo), four transcriptional Stops (STOP), and a EcoRI site, flanked by LoxP sites (arrowheads); (3) p53 exons, including the nonsense mutation in exon 10 (asterisk) and an additional Bcl I site; (4) a 2.8-kb-long 3′ homology region; and (5) the *diphtheria* α*-toxin* (DTA) gene for targeting enrichment. Recombinants from the depicted crossing-overs were identified by a 2.4-kb-long band after PCR with primers i and j, and bands of 2.1, 1.1, and 0.5 kb after PCR with primers g and h and Bcl I digestion. Recombinant clones were also analyzed by Southern blot with the indicated probe as containing a 10.5 kb EcoRI band. The mutation was routinely genotyped by PCR with primers e and f and Bcl I digestion.

(B–D) Screening of recombinant clones as described in (A). ES clones were screened (asterisk [*] indicates a positive clone) by PCR with primers i and j (B), with primers g and h, then PCR products were digested or not (b or u) with BclI (C) and by Southern blot (D).

(E) MEF genotyping by PCR. MEFs, prepared from embryos from an intercross of $p53^{+/LSL-\Delta31}$ mice, were genotyped by PCR with primers e and f followed by Bcl I digestion.

See also Figure S1.

$p53^{\Delta31/\Delta31}$ mice model DC, an archetypal telomere syndrome caused by mutations in genes encoding components of the telomerase or shelterin complexes, or telomerase regulators (Armanios and Blackburn, 2012). In support of this conclusion, $p53^{\Delta31/\Delta31}$ mice presented full-blown clinical features of DC: cutaneous hyperpigmentation, nail dystrophy, and oral leukoplakia (Figures 4E and 4F). Furthermore, the small size, hypogonadism, and cerebellar hypoplasia observed in some mice (Figures 3B, S4C, and S4D) characterize patients with the Hoyeraal-Hreidarsson syndrome (HHS), a severe variant of DC (Armanios and Blackburn, 2012).

DC-related features were also detected in $p53^{+/\Delta31}$ mice: three $p53^{+/\Delta31}$ mice died within a year with a hypertrophic heart (Figure 5A). Moreover, heterozygous mutants with lower levels of p53-negative regulators (i.e., most $p53^{+/\Delta31}$ $Mdm4^{+/-}$ and a few $p53^{+/\Delta31}$ $Mdm2^{+/-}$ mice) died within 3 months (Figure 5B). This suggested that the levels of p53 inhibitors—particularly Mdm4—impacted the severity of DC-related symptoms. Accordingly, bone marrow cellularity and telomere length were decreased in $p53^{+/\Delta31}$ $Mdm4^{+/-}$ mice compared to $p53^{+/\Delta31}$ mice (Figures 5C, 5D, and S6).

p53 Activation Alters the Expression of Genes Mutated in Telomere Syndromes

Animal models recently suggested that dysfunctional telomeres (Wang et al., 2011b) or altered ribosomal RNA processing (Pereboom et al., 2011) could lead to p53 activation and bone marrow failure. Our data suggested that a p53-truncating mutation might

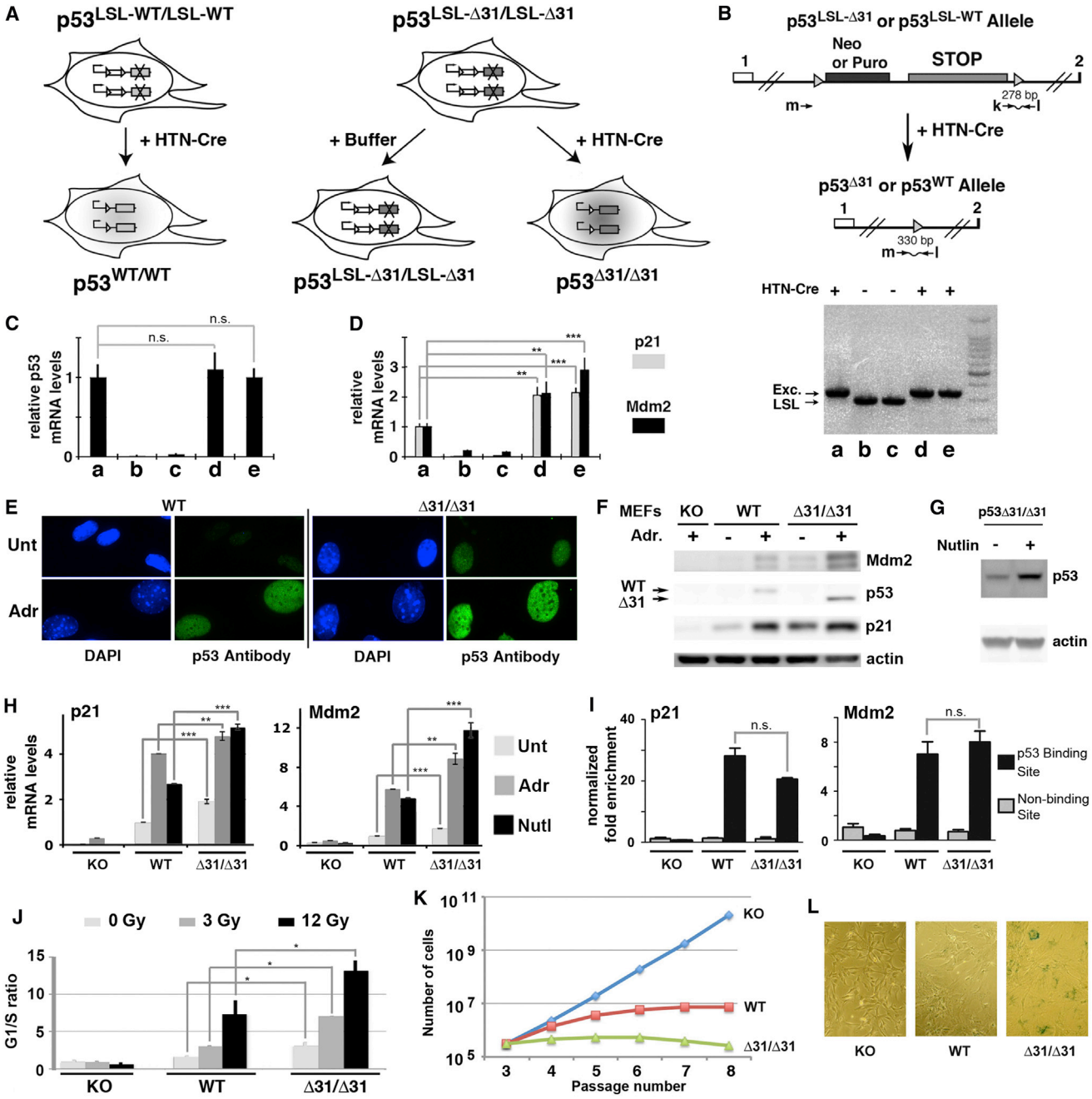

Figure 2. p53$^{\Delta 31/\Delta 31}$ MEFs Exhibit Increased p53 Activity

(A) Strategy to analyze the effects of an excision of the LSL cassette ex vivo. A His-tagged NLS-Cre recombinase (HTN-Cre) was added to p53$^{LSL\text{-}\Delta 31/LSL\text{-}\Delta 31}$ MEFs, allowing excision of the Stop cassette within 24 hr. p53$^{\Delta 31/\Delta 31}$ MEFs were then recovered and analyzed (right). As controls, p53$^{LSL\text{-}WT/LSL\text{-}WT}$ MEFs were treated likewise (left). p53$^{LSL\text{-}\Delta 31/LSL\text{-}\Delta 31}$ MEFs were also treated with a buffer solution devoid of Cre as negative controls (center).

(B) Efficiency of the Cre-mediated excision of the LSL cassette. LSL excision was determined using multiplex PCR with primers k, l, and m. Prior excision, a 278-bp-long product results from amplification with primers k and l, whereas primers m and l are too far apart to generate a PCR product. After excision, primers m and l generate a 330-bp-long product. The PCR analysis of the experiment described in (A) is shown: PCRs show ~100% efficiency in LSL excision (Exc.) in lanes a, d, and e; and 0% in lanes b and c.

(C and D) p53$^{LSL\text{-}\Delta 31/LSL\text{-}\Delta 31}$ MEFs exhibit increased p53 activity after LSL excision. mRNAs were prepared from p53$^{LSL\text{-}WT/LSL\text{-}WT}$ MEFs treated with HTN-Cre (a) or p53$^{LSL\text{-}\Delta 31/LSL\text{-}\Delta 31}$ MEFs treated with buffer (b and c) or HTN-Cre (d and e). p53 mRNAs (C) or p21 and Mdm2 mRNAs (D) were quantified using real-time PCR, normalized to control mRNAs, then the amount in (a) was assigned a value of 1.

(E–L) Comparative analysis of WT and p53$^{\Delta 31/\Delta 31}$ MEFs.

(E) WT and p53$^{\Delta 31/\Delta 31}$ (Δ31/Δ31) MEFs untreated (Unt) or treated with 0.5 μg/ml Adriamycin (Adr) for 24 hr were stained with a p53 antibody, and their DNA was counterstained with DAPI.

(legend continued on next page)

be sufficient to cause bone marrow failure but also typical DC features including short telomeres and oral leukoplakia (Table 1). Laboratory mice have long telomeres, and mice that lack telomerase exhibit short telomeres only after several generations of intracrosses (Blasco et al., 1997). However, mice with a telomerase haploinsufficiency and a deficient shelterin complex exhibit telomere dysfunction in a single generation (G1) (Hockemeyer et al., 2008; He et al., 2009). The short telomeres in G1 $p53^{\Delta31/\Delta31}$ mice thus suggested a pleiotropic effect of p53 on telomere metabolism.

Although p53 may regulate TRF2 via the ubiquitin ligase Siah1 (Fujita et al., 2010), a link between p53 and genes mutated in DC appeared most likely for *TCAB1/WRAP53* because this gene partially overlaps *TP53* (Zhong et al., 2011). However, we found no evidence of decreased Tcab1 expression in $p53^{\Delta31/\Delta31}$ cells (Figure 6A). We next quantified the mRNAs for nine other genes known to cause DC or implicated in aplastic anemia in $p53^{-/-}$, WT, and $p53^{\Delta31/\Delta31}$ cells and obtained evidence of modest but significant decreases in the expression of *Dyskerin* (*Dkc1*), *Rtel1*, *Tinf2*, and *Terf1* in $p53^{\Delta31/\Delta31}$ cells (Figures 6B and 6C). Consistent with this, p53 activation led to the downregulation of the four genes, with a stronger effect on *Dkc1* (Figure 6D).

Interestingly, mice in this study were of mixed genetic background (75% C57Bl/6J; 25% 129S2/SvPas). The coat color of inbred C57Bl/6J (B6) mice is black, whereas that of 129S2/SvPas (129) is agouti because these strains carry nonagouti (*a*) or agouti (A^w) alleles, respectively. We noticed that most $p53^{\Delta31/\Delta31}$ mice alive after 3 months (Figure 3A) had an agouti coat color and, conversely, that the few $p53^{+/\Delta31}$ mice that died in less than a year (Figure 5A) had a black coat color. These observations suggested that a gene physically linked to the A^w/a locus had an impact on the survival of $p53^{\Delta31}$ mutants and that the 129 allele for this gene correlated with a better survival. *Rtel1* appeared as a candidate gene because it is a dominant-positive regulator of telomere length (Ding et al., 2004) that maps 26 cM away from the A^w/a locus. We used a SNP within the *Rtel1* intron 15 (rs33116597) that differs between the B6 and 129 strains to genotype *Rtel1* alleles in a cohort of 52 $p53^{\Delta31/\Delta31}$ mice and found a significant increase in survival for $p53^{\Delta31/\Delta31}$ mice carrying 129 *Rtel1* allele(s) (Figures 6E and 6F). Importantly, when we quantified Rtel1 mRNA levels in BMCs of the C57Bl/6J and 129S2/SvPas pure inbred strains, we found increased levels in 129 cells (Figure 6G). Together, these results suggest that basal levels of Rtel1 mRNAs may affect the severity of phenotypes caused by the $p53^{\Delta31}$ mutation.

We next aimed to determine how p53 downregulates the *Dkc1*, *Rtel1*, *Tinf2*, and *Terf1* genes. Because p21 levels are known to contribute to the p53-mediated downregulation of many genes (Löhr et al., 2003), we tested if p53 could downregulate these genes in $p21^{-/-}$ MEFs. We found that p21 is required for the p53-mediated downregulation of *Rtel1*, *Tinf2*, and *Terf1*, but not *Dkc1* (Figure 6H). This suggested a more direct mechanism for the downregulation of *Dkc1*. Consistent with this, *Dkc1* was efficiently downregulated after treating WT cells with Nutlin for only 6 hr, whereas for the other genes, we observed a partial downregulation after 6–9 hr of Nutlin and a more efficient downregulation after 24 hr of Nutlin (Figure 6I). Furthermore, chromatin immunoprecipitation (ChIP) experiments provided direct evidence that p53 binds the *Dkc1* promoter (Figures 6J–6K).

In summary, we found that a nonsense mutation in the exon 10 of *Trp53*, encoding the truncated protein $p53^{\Delta31}$, causes an increase in p53 activity and phenotypes related to human telomere syndromes. To perform a more comprehensive analysis of nonsense mutations affecting *Trp53* exon 10, we also targeted in MEFs mutations encoding $p53^{\Delta36}$, $p53^{\Delta45}$, or $p53^{\Delta52}$ and found that only the latter two mutations led to measurable decreases in p53 mRNAs and activity (Figures S7A–S7G). Strikingly, the nonsense mutations affecting human *TP53* exon 10 that were reported in cancers also cause the loss of at least 45 residues, suggesting that our finding in mice might be relevant to humans (Figure S7H). Given that decreased dyskerin levels may cause short telomeres (Parry et al., 2011a), that Rtel is a major determinant of telomere length (Ding et al., 2004), and that mutations in *DKC1* or *RTEL1* are found in a significant fraction of patients with DC or HHS (Armanios and Blackburn, 2012; Ballew et al., 2013; Walne et al., 2013), it was important to test whether or not p53 downregulates these genes in human cells. We compared human primary WT cells with p53-deficient cells and observed that the activation of human p53 also leads to the downregulation of *DKC1* and *RTEL1* (Figures 6L and 6M). Our finding that p53 downregulates these genes in both species strengthens the notion that p53 plays a significant role in the regulation of telomere metabolism.

DISCUSSION

A Targeted Deletion of the p53 CTD Leads to Increased p53 Activity

In this report, we targeted a nonsense mutation at the murine *Trp53* locus to analyze the consequences of a deletion of the

(F) Protein extracts, prepared from indicated MEFs untreated or treated as in (E), were immunoblotted with antibodies against Mdm2, p53, p21, and actin. Band quantification revealed that unstressed $p53^{\Delta31/\Delta31}$ MEFs contained three to three and a half times more p21 or Mdm2 proteins than unstressed WT cells.
(G) $p53^{\Delta31/\Delta31}$ MEFs were untreated or treated with 10 μM Nutlin for 24 hr before protein extraction.
(H) mRNAs from indicated MEFs were quantified as in (C), and amounts in unstressed WT cells were assigned a value of 1. Nutl, Nutlin.
(I) ChIP assay was performed for p53-binding sites and nonbinding sites at the *p21* and *Mdm2* loci in Adriamycin-treated MEFs with an antibody against p53 phosphorylated serine 18 or rabbit IgG as a negative control. Immunoprecipitates were quantified using real-time PCR. Fold enrichments were normalized to data over an irrelevant region.
(J) Cell-cycle control was analyzed in asynchronous cell populations 24 hr after 0, 3, or 12 Gy γ-irradiation.
(K) $p53^{\Delta31}$ leads to a decreased proliferation capacity in a 3T3 protocol. The proliferation of $p53^{-/-}$ (KO), WT, and $p53^{\Delta31/\Delta31}$ (Δ31/Δ31) MEFs was compared. Each point is a mean value from two independent MEFs, the value for each MEF resulting from triplicate plates.
(L) Senescence-associated β-galactosidase staining of $p53^{-/-}$, WT, and $p53^{\Delta31/\Delta31}$ MEFs at passage 8.
Mean + SEM from three or more experiments are shown in all figures. ***$p \leq 0.001$; **$p \leq 0.01$; *$p \leq 0.05$; n.s., not significant by Student's t test.
See also Figure S2.

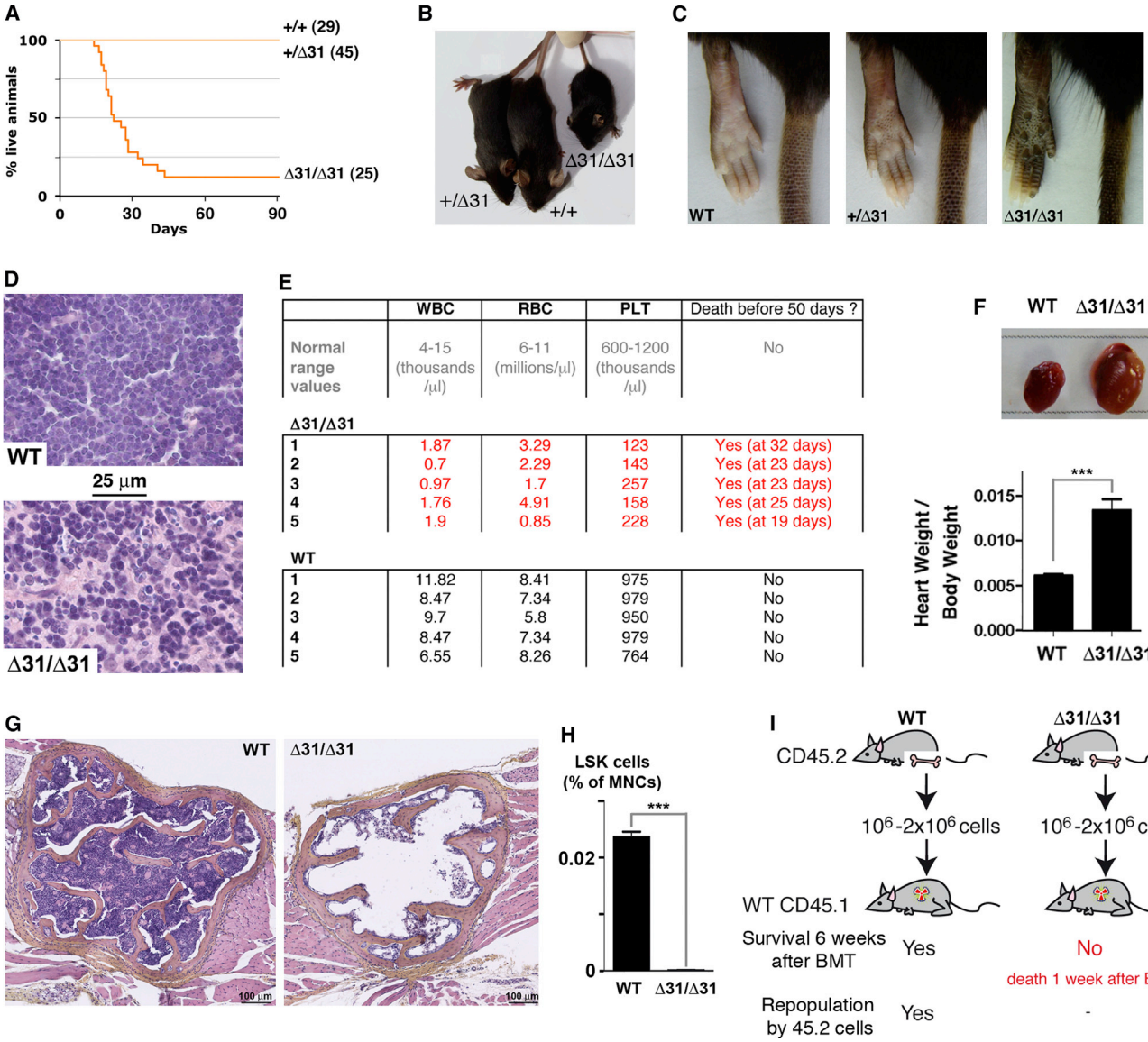

Figure 3. Increased p53 Activity and Aplastic Anemia in p53$^{\Delta 31/\Delta 31}$ Mice

(A) Survival of WT, p53$^{+/\Delta 31}$ (+/Δ31), and p53$^{\Delta 31/\Delta 31}$ (Δ31/Δ31) mice over 90 days. Cohort sizes are in parentheses.

(B) Examples of 28-day-old (P28) WT, p53$^{+/\Delta 31}$, and p53$^{\Delta 31/\Delta 31}$ littermates.

(C) Photographs of legs and tails of the same mice. Compared to the WT, the heterozygote has a slightly darker pigmentation of the palm and tail. The homozygote mutant has a much darker pigmentation, which includes footpads.

(D) Comparative analysis of hematoxylin and eosin staining (H&E) of the thymus of WT and mutant P23 littermates, showing an increased spontaneous apoptosis in the mutant.

(E–I) p53$^{\Delta 31/\Delta 31}$ mice suffer from aplastic anemia.

(E) Hemograms from p53$^{\Delta 31/\Delta 31}$ and WT mice. WBC, white blood cells; RBC, red blood cells; PLT, platelets. All mice were 3–4 weeks old when their hemogram was determined, except for mouse Δ31/Δ31 #5, moribund at 19 days, which was analyzed and euthanized on the same day.

(F) Mutant mice present enlarged hearts upon dissection. Top view shows example of hearts from WT and p53$^{\Delta 31/\Delta 31}$ P18 littermates. Bottom view illustrates heart/total body weight ratios determined for nine WT and ten p53$^{\Delta 31/\Delta 31}$ age-matched animals.

(G) H&E of sternum sections from WT and p53$^{\Delta 31/\Delta 31}$ P23 littermates.

(H) BMCs, stained with antibodies against hematopoietic lineage (Lin) markers and cell surface marks Sca1 and c-Kit, were analyzed by flow cytometry. The population of Lin− Sca1+ c-Kit+ (LSK) cells, enriched in hematopoietic stem cells, were calculated as percentage (%) of total mononucleated cells (MNCs). Results are from three mice per genotype.

(I) BMCs (1 or 2 × 10^6) from WT or p53$^{\Delta 31/\Delta 31}$ donor mice expressing the leukocyte marker CD45.2 were transplanted into lethally irradiated recipient mice (initially expressing marker CD45.1). Transplanted WT cells, but not p53$^{\Delta 31/\Delta 31}$ cells, rescued the irradiated animals by repopulating the bone marrow. Results are from five mice per genotype. BMT, bone marrow transplant.

Mean + SEM are shown in (F) and (H). *** $p \leq 0.001$, Student's t test.

See also Figures S3 and S4.

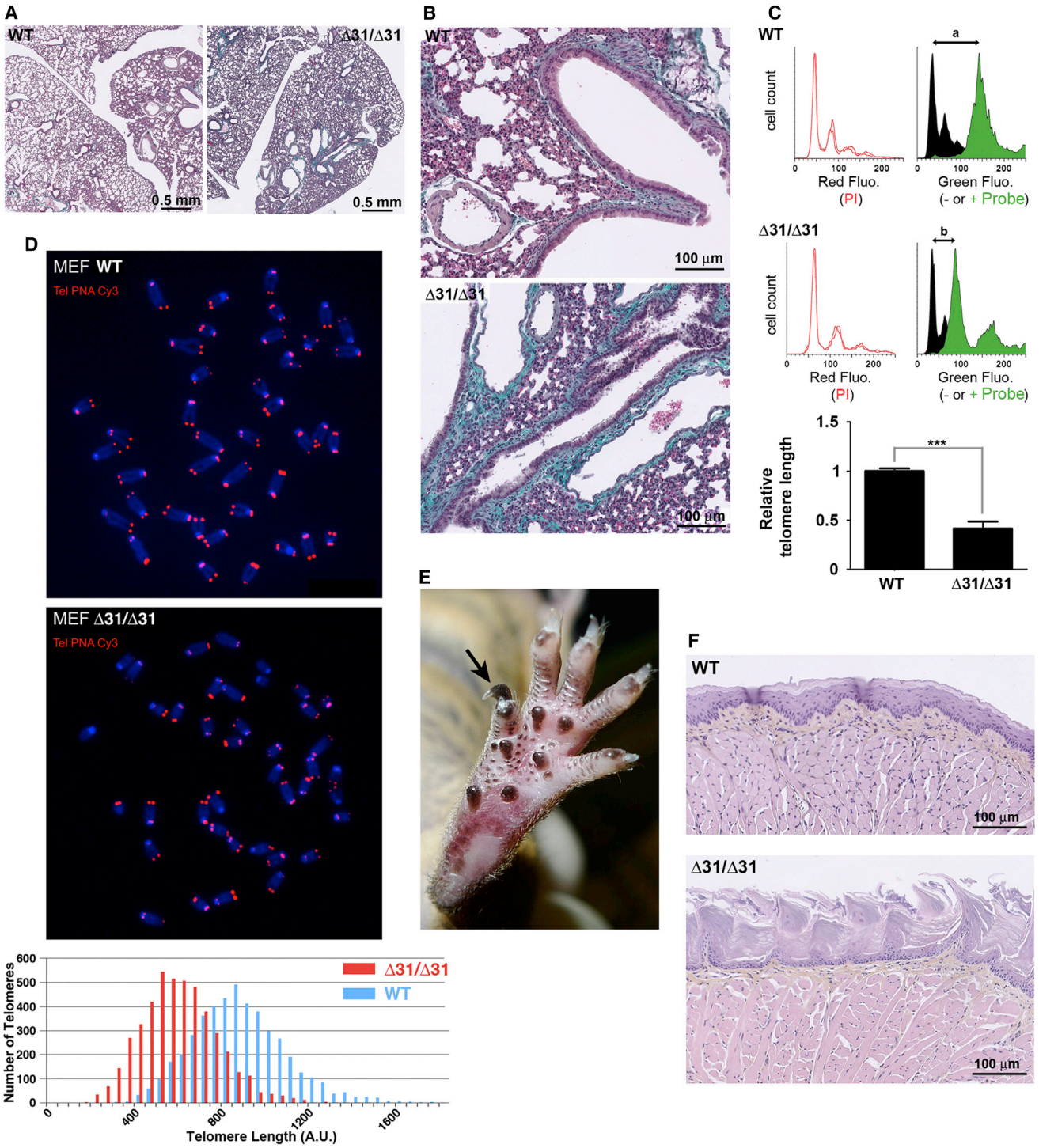

Figure 4. p53$^{\Delta 31/\Delta 31}$ Mice Exhibit Features Specific to DC

(A and B) Pulmonary fibrosis in p53$^{\Delta 31/\Delta 31}$ mice. Masson's trichrome staining of lungs from WT and p53$^{\Delta 31/\Delta 31}$ mice, shown at different magnifications. Interstitial fibrosis, characterized by deposits of collagen (stained in green), is increased in the mutant.

(C and D) p53$^{\Delta 31/\Delta 31}$ cells have short telomeres. In (C), telomere length was analyzed in BMCs using flow-FISH with a telomere-specific PNA probe. On top, typical results with P18 littermate mice are shown (>2,100 cells per sample, from a WT and a p53$^{\Delta 31/\Delta 31}$ mouse). For each animal, histograms on the right show green fluorescence (Fluo.), with black histograms for cells without the probe (measuring cellular autofluorescence), and green histograms for cells with the probe. The shift in fluorescence intensity is smaller in mutant cells (b < a), indicating reduced telomere length. Histograms on the left show propidium iodide fluorescence (superposed for cells with or without the probe). Bottom row presents results from four animals per genotype. Mean + SEM are shown. ***p $\leq$ 0.001, Student's

(legend continued on next page)

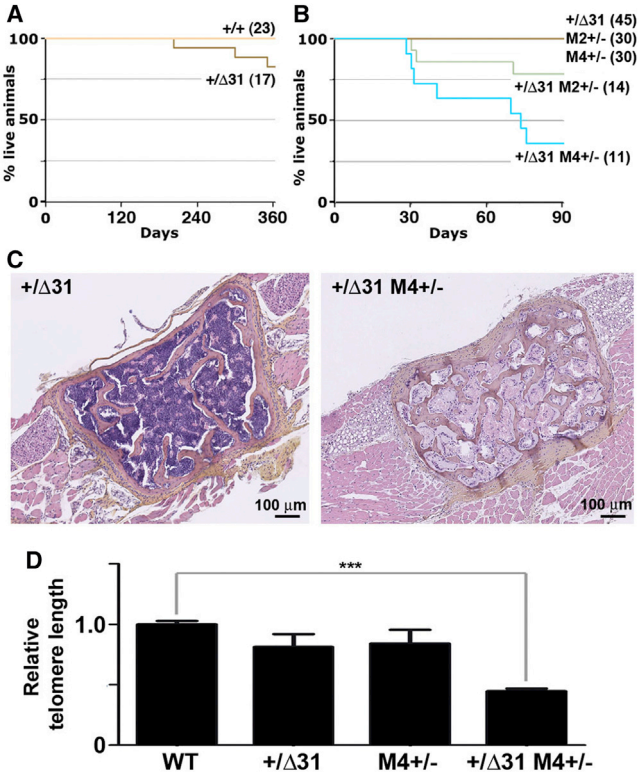

Figure 5. $p53^{+/\Delta31}$ Mice Are Extremely Sensitive to Mdm4 Levels

(A) Survival of WT (+/+) and $p53^{+/\Delta31}$ (+/Δ31) mice over 1 year, plotted as in Figure 3A.

(B) Survival of $p53^{+/\Delta31}$, $Mdm2^{+/-}$ (M2+/−), $Mdm4^{+/-}$ (M4+/−), $p53^{+/\Delta31}$ $Mdm2^{+/-}$ (+/Δ31 M2+/−), and $p53^{+/\Delta31}$ $Mdm4^{+/-}$ (+/Δ31 M4+/−) mice over 3 months.

(C) H&E of sternum sections from $p53^{+/\Delta31}$ and $p53^{+/\Delta31}$ $Mdm4^{+/-}$ littermates.

(D) Telomere length was measured by flow-FISH as described in Figure 4C, in BMCs from WT, $p53^{+/\Delta31}$, $Mdm4^{+/-}$, and $p53^{+/\Delta31}$ $Mdm4^{+/-}$ mice. Results are from three animals per genotype.

Mean + SEM are shown. ***$p \leq 0.001$, Student's t test.

See also Figure S6.

p53 C-terminal domain ex vivo and in vivo. The mutation led to increased $p53^{\Delta31}$ levels, consistent with in vitro studies that concluded that the p53 CTD is required for an optimal interaction between p53 and its ubiquitin ligase Mdm2 (Poyurovsky et al., 2010). Cells expressing $p53^{\Delta31}$ also exhibited increased p53 activity, despite the fact that the binding of the mutant protein to target gene promoters was not significantly increased. Thus, as earlier observations suggested (Kaeser and Iggo, 2002; Espinosa, 2008), the induction of a p53 target gene is not simply determined by the amount of p53 bound to its promoter. Presumably, the deletion of the p53 CTD might activate transcription by affecting p53-Mdm2 interactions (Poyurovsky et al., 2010) and/or by preventing the formation of p53 CTD-Mediator inactive complexes (Meyer et al., 2010).

Our observation that a p53 mutant lacking the CTD exhibits increased activity may seem surprising when compared to recent studies relying on ectopically expressed human p53 CTD mutants, which concluded that the CTD mainly acts as a positive regulator of p53 functions (Hamard et al., 2012; Kim et al., 2012). Importantly, however, these studies analyzed WT and mutant p53 expressed at equal levels, whereas we showed here that a targeted CTD deletion leads to mutant protein accumulation. In that respect, it is worth considering that despite its increased nuclear abundance, $p53^{\Delta31}$ did not exhibit an increased binding at p53 target gene promoters. This may suggest that, on a per molecule basis, $p53^{\Delta31}$ is less efficient than WT p53 for sequence-specific DNA binding, consistent with other studies (McKinney et al., 2004; Tafvizi et al., 2011). Therefore, it appears likely that if $p53^{\Delta31}$ had been expressed at similar levels than WT p53 in the mutant cells, the overall increase in p53 activity would not have been observed. Our observations thus suggest that differences in expression levels might underlie much of the contradictions in the p53 CTD literature.

p53 Mutations Affecting the CTD Model Telomere Syndromes

Germline missense *TP53* mutations affecting the core DNA-binding domain are well known to cause the cancer-prone Li-Fraumeni syndrome in humans (Malkin et al., 1990; Srivastava et al., 1990), and mice with equivalent p53 mutations may, like patients with Li-Fraumeni, develop osteosarcomas (Lang et al., 2004; Olive et al., 2004). In striking contrast, we found here that mice homozygous for a germline nonsense mutation affecting the p53 CTD, or compound heterozygotes with a Mdm4 haploinsufficiency, are remarkable models of human telomere syndromes. In murine cells, p53 activation led to the downregulation of four genes including *Dyskerin* (*Dkc1*), a gene often mutated in patients with DC (Armanios and Blackburn, 2012). Importantly, in addition to its role as a telomerase component, dyskerin acts as a pseudouridine synthase in snoRNP complexes. This might explain why patients with DC carrying *DKC1* mutations exhibit more clinical features than patients carrying *TERC* mutations (Vulliamy et al., 2011). Similarly, some of the DC features observed in $p53^{\Delta31/\Delta31}$ mice might result from p53 activation or *Dkc1* downregulation, rather than telomere dysfunction per se. However, decreased telomere length likely played a role in the premature death of $p53^{\Delta31/\Delta31}$ mice because we found strain-specific differences in Rtel1 mRNA levels to correlate with differences in the survival of mutant mice.

t test. In (D), telomere length was analyzed in WT or $p53^{\Delta31/\Delta31}$ MEFs at passage 5 by quantitative FISH with a telomere-specific Cy3 PNA probe (in red). On top, typical metaphases are shown. In the mutant cells, several chromosomes exhibit faint or no visible telomeric signals. Below, quantification results from an analysis of 28 metaphases per genotype are shown.

(E and F) $p53^{\Delta31/\Delta31}$ mice exhibit the triad of physical traits classically used to diagnose DC.

(E) Cutaneous hyperpigmentation and nail dystrophy on a $p53^{\Delta31/\Delta31}$ hindleg. Arrow points to the dystrophic nail.

(F) H&E comparison of the dorsal surface of a WT and a $p53^{\Delta31/\Delta31}$ tongue. The mutant tongue exhibits acanthosis and hyperparakeratosis, typical of oral leukoplakia.

See also Figure S5.

Table 1. Features of DC in $p53^{\Delta31/\Delta31}$ Mice and in Other Reported Mice with Altered p53 Regulation or Dysfunctional Telomeres

Clinical Features in Patients Diagnosed with DC	Observed in $p53^{\Delta31/\Delta31}$ Mice % Animals with Feature (No. Analyzed)	Observed in Other Mice with Altered p53 Regulation[a]	Observed in Mouse Models of DC[b]
Physical Traits (Diagnostic Triad)[c]			
Skin hyperpigmentation	**✓ 100% (25)**	**✓**	**✓**
Nail dystrophy	**✓ 8% (25)**	**Not reported**	**✓**
Oral leukoplakia	**✓ 100% (8)**	**Not reported**	**Not reported**
Pathological Traits[d]			
Bone marrow failure	**✓ 100% (8)**	**✓**	**✓**
Pulmonary fibrosis	**✓ 87% (8)**	**Not reported**	**Not reported**
Molecular Feature[e]			
Poor telomere maintenance	**✓ 100% (4)**	**Not reported**	**✓**
Associated Features[f]			
Hypertrophic heart	✓ 100% (25)	✓	Not reported
Short stature	✓ 63% (25)	✓	✓
Testicular atrophy	✓ 91% (11)	✓	✓
Cerebellar hypoplasia	✓ 30% (10)	✓	Not reported

The features used to diagnose DC are indicated in bold. $p53^{+/\Delta31}$ $Mdm4^{+/-}$ mice, not included in this table, exhibited the same features as $p53^{\Delta31/\Delta31}$ mice. Likewise, $p53^{\Delta31/\Delta31}$ MEFs exhibited short/dysfunctional telomeres but were not included in this table.

[a]Mice with altered p53 regulation include mutants with severe decreases in Mdm2 levels (Mendrysa et al., 2003; Liu et al., 2007), combined Mdm2 and Mdm4 haploinsufficiencies (Terzian et al., 2007), complex p53 mutations (McGowan et al., 2008; Liu et al., 2010; Wang et al., 2011a), or constitutive cellular stress (McGowan et al., 2008).

[b]Previously reported mouse models of DC combined a Pot1b deficiency with a telomerase RNA haploinsufficiency (Hockemeyer et al., 2008; He et al., 2009).

[c]DC is classically diagnosed when at least two of these physical features are observed.

[d]Inherited bone marrow failure is found in other syndromes (e.g., Blackfan-Diamond anemia, Fanconi anemia), but the combination of bone marrow failure and pulmonary fibrosis characterizes DC (Parry et al., 2011b).

[e]Telomeres are often analyzed to diagnose DC.

[f]These features can be found in patients with DC but are not specific enough for diagnosis.

Importantly, $p53^{+/\Delta31}$ mice were mildly affected: they presented only slight alterations (if any) in HSC pools and telomere length, and most were alive for more than 12 months. Because $p53^{\Delta31/\Delta31}$ and $p53^{+/\Delta31}$ $Mdm4^{+/-}$ mice developed full-blown DC features, we conclude that a $\leq$2-fold difference in p53 activity was sufficient to prevent the observation of DC features in heterozygous mice. This observation might explain why mouse models with modest increases in p53 activity were only found to present slight alterations in HSC pools (e.g., Herrera-Merchan et al., 2010).

An important remaining question is whether germline p53 mutations affecting the CTD may lead to telomere syndromes in humans. The high degree of conservation between the human and murine p53 CTDs, the comparison of phenotypes caused by nonsense mutations in the exon 10 of the human and mouse p53 genes, and the fact that p53 activation also leads to the downregulation of *DKC1* and *RTEL1* in human cells together support this possibility. Importantly, genes presently known to cause DC account for about only half of the clinical cases, and patients with DC are now thought to represent a small fraction of persons suffering from a telomere syndrome (Armanios and Blackburn, 2012). Although one should be careful about extrapolating mouse data to human diseases, our results lead us to propose that *TP53* (and possibly *MDM4*) should be sequenced in patients with telomere syndromes of currently unknown molecular origin.

EXPERIMENTAL PROCEDURES

Cells and Cell Culture Reagents

MEFs isolated from 13.5-day embryos were cultured in a 5% CO_2 and 3% O_2 incubator, in DMEM GlutaMAX (Gibco), with 15% FBS (Biowest), 100 μM 2-mercaptoethanol (Millipore), 0.01 mM Non-Essential Amino-Acids, and penicillin/streptavidin (Gibco) for six or less passages, except for 3T3 experiments, performed in a 5% CO_2 incubator for eight passages. Human lung fibroblast MRC5 and its SV40-transformed derivatives were cultured in a 5% CO_2 and 3% O_2-regulated incubator in MEM (Gibco), completed with 10% FBS, 2 mM L-glutamine (Gibco), 1 mM pyruvate, 10 μM Non-Essential Amino-Acids, and penicillin/streptomycin. Cells were irradiated with a Cs γ-irradiator or treated with Adriamycin (Sigma-Aldrich) at 0.5 μg/ml or 10 μM Nutlin 3a (Sigma-Aldrich).

Quantitative RT-PCR

Total RNA, extracted using NucleoSpin RNA II (Macherey-Nagel), was reverse transcribed using SuperScript III (Invitrogen). Real-time quantitative PCRs (primers available upon request) were performed on an ABI PRISM 7500 using Power SYBR Green (Applied Biosystems). For strain-specific Rtel1 expression analysis, total mRNAs were extracted from the BMCs of inbred C57Bl/6J and 129S2/SvPas mice (Charles River Laboratories), and Rtel1 mRNAs were quantified as above.

LSL-Δ31 Construct

We used mouse genomic p53 DNA from previous constructs (Toledo et al., 2006a, 2006b) and a portion of intron 1 containing a LoxP-Stop-LoxP (LSL) cassette (Ventura et al., 2007) in which the *puromycin*-resistance gene was replaced by a *neomycin* gene (details available upon request). A BsrG I site (in intron 9) and a Fse I site (inserted downstream *Trp53*) were used to swap

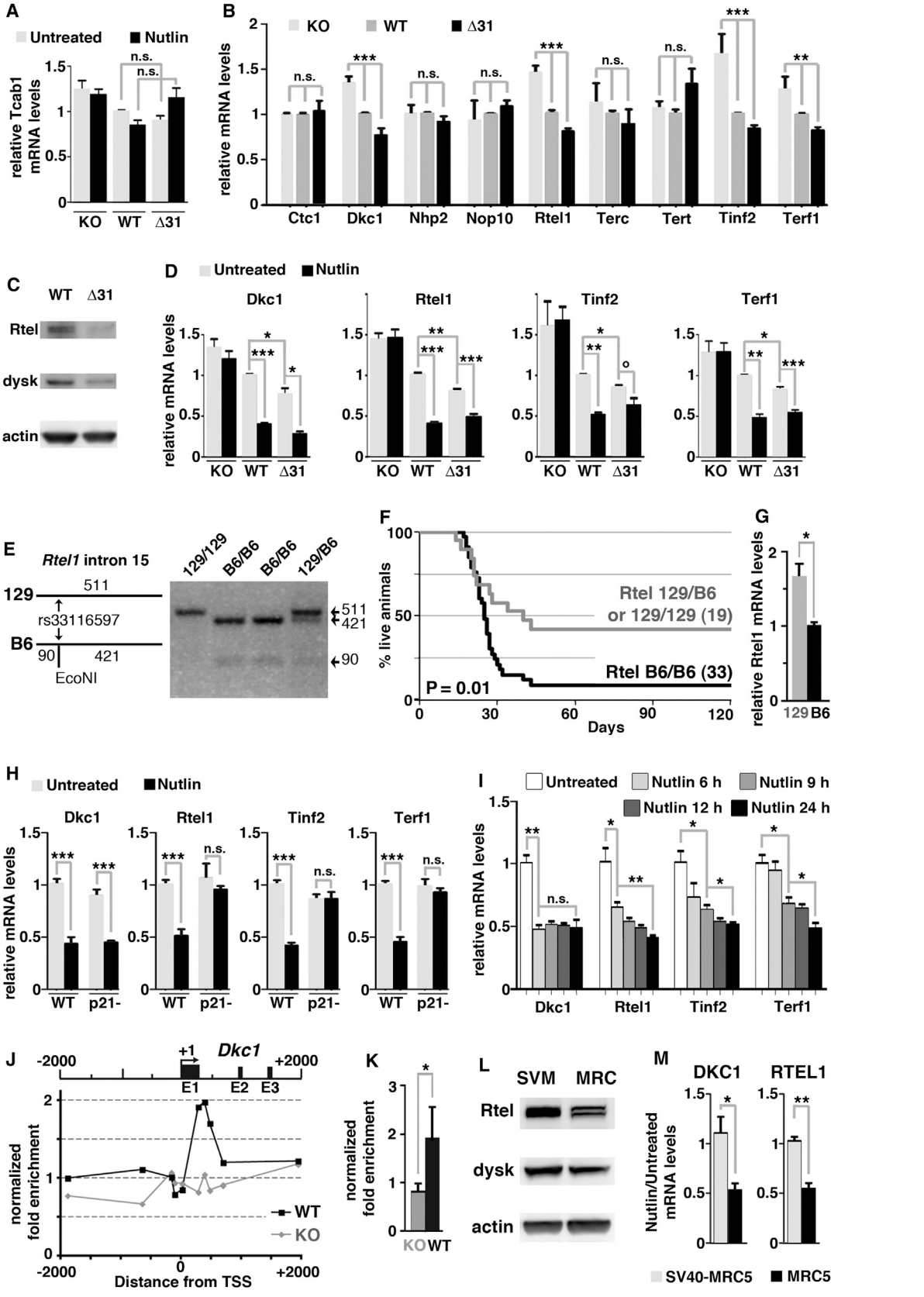

(legend on next page)

the nonsense mutation from the $p53^{\Delta 31}$ RMCE-ASAP construct (Extended Experimental Procedures) in the LSL-targeting construct. The resulting LSL-$p53^{\Delta 31}$-targeting vector was fully sequenced before use.

Targeting in ES Cells and Genotyping

CK-35 ES cells were electroporated with the targeting construct linearized with Not I. Two independent recombinant clones, identified by long-range PCR and confirmed by Southern blot and PCR, were injected into blastocysts to generate chimeras, and germline transmission was verified by genotyping MEFs from their offspring. RT-PCR of RNAs from $p53^{LSL\text{-}\Delta 31/LSL\text{-}\Delta 31}$ MEFs treated with HTN-Cre showed that the mutant cDNA differed from a $p53^{WT}$ sequence only by the engineered nonsense mutation. Primers for *Trp53* and *Rtel1* genotyping are available upon request. All experiments were performed according to IACUC regulations.

LSL Cassette Excision

Triplicates of 1.8×10^5 $p53^{LSL\text{-}WT/LSL\text{-}WT}$ (Ventura et al., 2007) and $p53^{LSL\text{-}\Delta 31/LSL\text{-}\Delta 31}$ MEFs were seeded in wells of a 6-well plate and treated with 10 μM HTN-Cre for ex vivo excision of the LSL cassette or 10^5 cells with buffer only. After 24 hr, wells were washed, and cells were frozen when reaching 90% confluence. Cells were then thawed for DNA and RNA extractions to determine excision efficiency and for mRNA quantifications. In vivo LSL excision was performed by breeding with PGK-Cre mice.

Immunofluorescence

MEFs were cultured on collagen-coated coverslips, exposed to Adriamycin, and analyzed 24 hr later. Coverslips were stained with the p53 antibody CM-5 (Novocastra) and secondary Alexa Fluor 488 anti-mouse antibody (Molecular Probes). Images were captured on an epifluorescence microscope using equal exposure times for all images for each fluor.

Western Blots

Protein detection by immunoblotting was performed using antibodies against p53 (CM-5, Novocastra; or FL-393, Santa Cruz Biotechnology), actin (A2066; Sigma-Aldrich), p21 (F5; Santa Cruz Biotechnology), and Mdm2 (4B2), Rtel1 (MP1), and Dyskerin (H-300; Santa Cruz Biotechnology). Chemiluminescence revelation was achieved with SuperSignal West Dura (Perbio). Bands of interest were quantified by using ImageJ and normalized with actin.

ChIP Assay

ChIP analysis was performed as described (Simeonova et al., 2012). p53-DNA complexes were immunoprecipitated from total extracts by using 5 μg of an antibody against mouse Phospho-p53 Ser18 (Cell Signaling Technology) and 15–30 μg of sonicated chromatin, or 50 μg of a polyclonal antibody against p53 (FL-393) and 300 μg of sonicated chromatin. Rabbit IgG (Abcam) was used for control precipitation. Quantitative PCR was performed on ABI PRISM 7500.

Cell-Cycle Assays

Log phase cells were irradiated at RT with a Cs γ-irradiator at doses of 3 or 12 Gy, incubated for 24 hr, then pulse labeled for 1 hr with BrdU (10 μM), fixed in 70% ethanol, double stained with FITC anti-BrdU and propidium iodide, and sorted by using a BD Biosciences FACSort. Data were analyzed using FlowJo.

Anatomopathology

Organs were fixed in formol 4% for 24 hr, then ethanol 70%, and embedded in paraffin wax. Serial sections were stained with hematoxylin and eosin or Masson's trichrome using standard procedures (Prophet et al., 1992).

Figure 6. p53 Activation Leads to the Downregulation of Genes Involved in Telomere Metabolism

(A) Tcab1 mRNA levels are not altered in $p53^{\Delta 31/\Delta 31}$ cells. RNAs, prepared from $p53^{-/-}$ (KO), WT, and $p53^{\Delta 31/\Delta 31}$ (Δ31) MEFs, untreated or treated with 10 μM Nutlin for 24 hr, were used to quantify Tcab1/Wrap53 mRNAs. Results are from four independent experiments.

(B) Evidence of decreased mRNA levels for Dkc1, Rtel1, Tinf2, and Terf1 in unstressed $p53^{\Delta 31/\Delta 31}$ cells. RNAs, prepared from unstressed $p53^{-/-}$, WT, and $p53^{\Delta 31/\Delta 31}$ MEFs, were used to compare the expression of eight genes known to cause DC (*Ctc1*, *Dkc1*, *Nhp2*, *Nop10*, *Rtel1*, *Terc*, *Tert*, and *Tinf2*) and one gene (*Terf1*) that has been implicated in aplastic anemia, a milder form of telomere syndrome (Armanios and Blackburn, 2012). Results from four independent experiments were analyzed by one-way ANOVA.

(C) $p53^{\Delta 31/\Delta 31}$ cells contain decreased levels of the dyskerin and Rtel proteins. Protein extracts, prepared from WT and $p53^{\Delta 31/\Delta 31}$ MEFs, were immunoblotted with antibodies against Rtel, dyskerin (dysk), and actin.

(D) *Dkc1*, *Rtel1*, *Tinf2*, and *Terf1* are downregulated by murine p53. mRNAs for Dkc1, Rtel1, Tinf2, and Terf1 were quantified in $p53^{-/-}$, WT, and $p53^{\Delta 31/\Delta 31}$ MEFs, untreated or treated with 10 μM Nutlin for 24 hr. Results are from four independent experiments. °p = 0.0545.

(E–G) Improved survival of $p53^{\Delta 31/\Delta 31}$ mice carrying 129S2/SvPas *Rtel1* allele(s).

(E) DNA was extracted from 52 $p53^{\Delta 31/\Delta 31}$ mice of mixed genetic background, then PCR was performed with primers flanking the SNP rs33116597, and products were digested with EcoNI to genotype 129S2/SvPas (129) and C57Bl/6J (B6) *Rtel1* alleles because only the B6 PCR products contained an EcoNI site. A typical analysis of four mice is shown, with *Rtel1* genotypes above the gel.

(F) Survival of $p53^{\Delta 31/\Delta 31}$ mice taking *Rtel1* genotyping into account. Cohort sizes are in parentheses. The p value is from a log rank test.

(G) Comparison of Rtel1 mRNA levels in the BMCs of 129S2/SvPas (129) and C57Bl/6J (B6) mice. Results are from four mice per strain.

(H) p21 is required for the downregulation of *Rtel1*, *Tinf2*, and *Terf1*. RNAs, prepared from WT and $p21^{-/-}$ (p21−) MEFs, untreated or treated with 10 μM Nutlin for 24 hr, were used to quantify Dkc1, Rtel1, Tinf2, and Terf1 mRNAs. Results are from three independent experiments.

(I) p53 activation rapidly leads to the efficient downregulation of *Dkc1*. mRNAs for Dkc1, Rtel1, Tinf2, and Terf1 were quantified in WT MEFs, untreated or treated with 10 μM Nutlin for 6, 9, 12, or 24 hr. Results are from two independent experiments.

(J and K) p53 regulates the *Dkc1* promoter.

(J) ChIP assay was performed at ten different sites surrounding the Dkc1 mRNA transcription start site (TSS) in Adriamycin-treated WT and $p53^{-/-}$ (KO) MEFs by using a polyclonal antibody against p53 (FL-393) or rabbit IgG as a negative control. Immunoprecipitates were quantified using real-time PCR. Fold enrichments were normalized to data over an irrelevant region. Indicated values are means from two independent ChIP experiments, each quantified in triplicates. Results suggest p53 binding near the end of exon 1 (E1) of *Dkc1*.

(K) Data from three independent ChIP experiments focusing on the end of *Dkc1* exon 1 confirm significant p53 binding.

(L and M) Dyskerin and Rtel are also downregulated by p53 in human cells.

(L) Protein extracts, prepared from WT MRC5 human cells (MRC) and p53-deficient SV40-MRC5 cells (SVM), were immunoblotted with antibodies against Rtel, dyskerin, and actin.

(M) mRNAs were prepared from SV40-MRC5 and MRC5 human cells, untreated or treated with Nutlin, then DKC1 and RTEL1 mRNAs were quantified using real-time PCR, normalized to control mRNAs, and mRNA ratios from Nutlin-treated versus untreated cells were determined. Results from three independent experiments.

Mean + SEM are shown. ***$p \leq 0.001$; **$p \leq 0.01$; *$p \leq 0.05$; n.s., not significant by Student's t test.

See also Figure S7.

Hemograms

For each animal, 100 μl of blood was recovered retro-orbitally in a 10 μl citrate-concentrated solution (S5770; Sigma-Aldrich) and analyzed using a MS9 machine (Melet Schloesing Laboratory).

Hematopoietic Marker Analysis

BMCs were flushed from femurs and tibias of age-matched WT and $p53^{\Delta 31/\Delta 31}$ mice, then incubated with FITC-labeled antibodies against markers Gr1, B220, Ter119, TCR, CD19, Dx5, CD11b, CD4, and CD8, PE-conjugated anti-Sca1 and APC-conjugated anti-CD117, then analyzed using FlowJo.

Long-Term Reconstitution Assay

Donor BMCs were isolated from WT or $p53^{\Delta 31/\Delta 31}$ littermate mice (Ly5.2) and retro-orbitally injected into lethally irradiated Ly5.1 recipients, 4 hr post 12 Gy irradiation. Six weeks posttransplant, reconstitution of donor leukocytes was analyzed by staining blood cells with antibodies against leukocyte cell surface markers CD45.1 (BD PharMingen) and CD45.2 (BioLegend) and flow cytometry.

Telomeric Flow-FISH

Flow-FISH was performed as described by Baerlocher et al. (2006). For each animal, the bone marrow from two tibias and two femurs was collected, red blood cells were lysed, then 2×10^6 cells were fixed in 500 μl PNA hybridization buffer (70% deionized formamide, 20 mM Tris [pH 7.4], 0.1% Blocking reagent; Roche) and stored at −20°C. Either nothing (control) or 5 μl probe stock solution was added to cells (probe stock solution: 10 μM TelC-FAM PNA probe [PANAGENE], 70% formamide, 20 mM Tris [pH 7.4]), and samples were denatured for 10 min at 80°C before hybridization for 2 hr at RT. After three washes, cells were resuspended in PBS 1×, 0.1% BSA, RNase A 1,000 U/ml, propidium iodide 12.5 μg/ml, and analyzed with a FACSCalibur.

Telomeric Quantitative FISH

Cells were treated with 0.5 μg/ml colcemide for 1.5 hr, submitted to hypotonic shock, fixed in a (3:1) ethanol/acetic acid solution, and dropped onto glass slides. Q-FISH was then carried out as described (Ourliac-Garnier and Londoño-Vallejo, 2011) with a TelC-Cy3 PNA probe (PANAGENE). Images were acquired using a Zeiss Axioplan 2, and telomeric signals were quantified with iVision (Chromaphor).

Statistical Analyses

The Student's t test was used in all figures to analyze differences between two groups of values. In Figure 6B, differences among three groups were analyzed by one-way ANOVA. In Figure 6F, a log rank test was used to analyze survival curves. Analyses were performed by using GraphPad Prism, and values of $p \leq 0.05$ were considered significant.

SUPPLEMENTAL INFORMATION

Supplemental Information includes Extended Experimental Procedures and seven figures and can be found with this article online at http://dx.doi.org/10.1016/j.celrep.2013.05.028.

LICENSING INFORMATION

ACKNOWLEDGMENTS

We thank I. Grandjean, C. Daviaud, and M. Garcia from the Animal Facility, C. Alberti, E. Belloir, and N. Mebirouk from the Transgenesis Platform, M. Richardson and A. Nicolas from the Pathology Service, and Z. Maciorowski from the Cell-Sorting Facility of the Institut Curie. We also thank M. Schertzer for technical advice and G.M. Wahl and M. Debatisse for their support. The "Genetics of Tumor Suppression" laboratory received funding from the Fondation de France (Comité Tumeurs), the Ligue Nationale contre le Cancer (Comité Ile de France), the Association pour la Recherche sur le Cancer, and the Institut National du Cancer. The "Telomeres and Cancer" laboratory is an "équipe labellisée" by the Ligue Nationale contre le Cancer. PhD students were supported by fellowships from the Ministère de l'Enseignement Supérieur et de la Recherche (to I.S. and S.J.), the Cancéropôle Ile de France (to M.F.), and the Ligue Nationale Contre le Cancer (to I.S. and M.F.).

Received: December 20, 2012
Revised: April 1, 2013
Accepted: May 17, 2013
Published: June 13, 2013

REFERENCES

Arai, N., Nomura, D., Yokota, K., Wolf, D., Brill, E., Shohat, O., and Rotter, V. (1986). Immunologically distinct p53 molecules generated by alternative splicing. Mol. Cell. Biol. *6*, 3232–3239.

Armanios, M., and Blackburn, E.H. (2012). The telomere syndromes. Nat. Rev. Genet. *13*, 693–704.

Baerlocher, G.M., Vulto, I., de Jong, G., and Lansdorp, P.M. (2006). Flow cytometry and FISH to measure the average length of telomeres (flow FISH). Nat. Protoc. *1*, 2365–2376.

Ballew, B.J., Yeager, M., Jacobs, K., Giri, N., Boland, J., Burdett, L., Alter, B.P., and Savage, S.A. (2013). Germline mutations of regulator of telomere elongation helicase 1, RTEL1, in Dyskeratosis congenita. Hum. Genet. *132*, 473–480.

Blasco, M.A., Lee, H.W., Hande, M.P., Samper, E., Lansdorp, P.M., DePinho, R.A., and Greider, C.W. (1997). Telomere shortening and tumor formation by mouse cells lacking telomerase RNA. Cell *91*, 25–34.

Brady, C.A., and Attardi, L.D. (2010). p53 at a glance. J. Cell Sci. *123*, 2527–2532.

Bruins, W., Zwart, E., Attardi, L.D., Iwakuma, T., Hoogervorst, E.M., Beems, R.B., Miranda, B., van Oostrom, C.T., van den Berg, J., van den Aardweg, G.J., et al. (2004). Increased sensitivity to UV radiation in mice with a p53 point mutation at Ser389. Mol. Cell. Biol. *24*, 8884–8894.

Ding, H., Schertzer, M., Wu, X., Gertsenstein, M., Selig, S., Kammori, M., Pourvali, R., Poon, S., Vulto, I., Chavez, E., et al. (2004). Regulation of murine telomere length by Rtel: an essential gene encoding a helicase-like protein. Cell *117*, 873–886.

Dumble, M., Moore, L., Chambers, S.M., Geiger, H., Van Zant, G., Goodell, M.A., and Donehower, L.A. (2007). The impact of altered p53 dosage on hematopoietic stem cell dynamics during aging. Blood *109*, 1736–1742.

Espinosa, J.M. (2008). Mechanisms of regulatory diversity within the p53 transcriptional network. Oncogene *27*, 4013–4023.

Feng, L., Lin, T., Uranishi, H., Gu, W., and Xu, Y. (2005). Functional analysis of the roles of posttranslational modifications at the p53 C terminus in regulating p53 stability and activity. Mol. Cell. Biol. *25*, 5389–5395.

Foord, O.S., Bhattacharya, P., Reich, Z., and Rotter, V. (1991). A DNA binding domain is contained in the C-terminus of wild type p53 protein. Nucleic Acids Res. *19*, 5191–5198.

Fujita, K., Horikawa, I., Mondal, A.M., Jenkins, L.M., Appella, E., Vojtesek, B., Bourdon, J.C., Lane, D.P., and Harris, C.C. (2010). Positive feedback between p53 and TRF2 during telomere-damage signalling and cellular senescence. Nat. Cell Biol. *12*, 1205–1212.

Hamard, P.J., Lukin, D.J., and Manfredi, J.J. (2012). p53 basic C terminus regulates p53 functions through DNA binding modulation of subset of target genes. J. Biol. Chem. *287*, 22397–22407.

He, H., Wang, Y., Guo, X., Ramchandani, S., Ma, J., Shen, M.F., Garcia, D.A., Deng, Y., Multani, A.S., You, M.J., and Chang, S. (2009). Pot1b deletion and telomerase haploinsufficiency in mice initiate an ATR-dependent DNA damage response and elicit phenotypes resembling dyskeratosis congenita. Mol. Cell. Biol. *29*, 229–240.

Herrera-Merchan, A., Cerrato, C., Luengo, G., Dominguez, O., Piris, M.A., Serrano, M., and Gonzalez, S. (2010). miR-33-mediated downregulation of p53 controls hematopoietic stem cell self-renewal. Cell Cycle *9*, 3277–3285.

Hockemeyer, D., Palm, W., Wang, R.C., Couto, S.S., and de Lange, T. (2008). Engineered telomere degradation models dyskeratosis congenita. Genes Dev. *22*, 1773–1785.

Hupp, T.R., Meek, D.W., Midgley, C.A., and Lane, D.P. (1992). Regulation of the specific DNA binding function of p53. Cell *71*, 875–886.

Kaeser, M.D., and Iggo, R.D. (2002). Chromatin immunoprecipitation analysis fails to support the latency model for regulation of p53 DNA binding activity in vivo. Proc. Natl. Acad. Sci. USA *99*, 95–100.

Kim, H., Kim, K., Choi, J., Heo, K., Baek, H.J., Roeder, R.G., and An, W. (2012). p53 requires an intact C-terminal domain for DNA binding and transactivation. J. Mol. Biol. *415*, 843–854.

Krummel, K.A., Lee, C.J., Toledo, F., and Wahl, G.M. (2005). The C-terminal lysines fine-tune P53 stress responses in a mouse model but are not required for stability control or transactivation. Proc. Natl. Acad. Sci. USA *102*, 10188–10193.

Lane, D., and Levine, A. (2010). p53 Research: the past thirty years and the next thirty years. Cold Spring Harb. Perspect. Biol. *2*, a000893.

Lang, G.A., Iwakuma, T., Suh, Y.A., Liu, G., Rao, V.A., Parant, J.M., Valentin-Vega, Y.A., Terzian, T., Caldwell, L.C., Strong, L.C., et al. (2004). Gain of function of a p53 hot spot mutation in a mouse model of Li-Fraumeni syndrome. Cell *119*, 861–872.

Liu, G., Terzian, T., Xiong, S., Van Pelt, C.S., Audiffred, A., Box, N.F., and Lozano, G. (2007). The p53-Mdm2 network in progenitor cell expansion during mouse postnatal development. J. Pathol. *213*, 360–368.

Liu, D., Ou, L., Clemenson, G.D., Jr., Chao, C., Lutske, M.E., Zambetti, G.P., Gage, F.H., and Xu, Y. (2010). Puma is required for p53-induced depletion of adult stem cells. Nat. Cell Biol. *12*, 993–998.

Löhr, K., Möritz, C., Contente, A., and Dobbelstein, M. (2003). p21/CDKN1A mediates negative regulation of transcription by p53. J. Biol. Chem. *278*, 32507–32516.

Malkin, D., Li, F.P., Strong, L.C., Fraumeni, J.F., Jr., Nelson, C.E., Kim, D.H., Kassel, J., Gryka, M.A., Bischoff, F.Z., Tainsky, M.A., et al. (1990). Germ line p53 mutations in a familial syndrome of breast cancer, sarcomas, and other neoplasms. Science *250*, 1233–1238.

McGowan, K.A., Li, J.Z., Park, C.Y., Beaudry, V., Tabor, H.K., Sabnis, A.J., Zhang, W., Fuchs, H., de Angelis, M.H., Myers, R.M., et al. (2008). Ribosomal mutations cause p53-mediated dark skin and pleiotropic effects. Nat. Genet. *40*, 963–970.

McKinney, K., Mattia, M., Gottifredi, V., and Prives, C. (2004). p53 linear diffusion along DNA requires its C terminus. Mol. Cell *16*, 413–424.

Mendrysa, S.M., McElwee, M.K., Michalowski, J., O'Leary, K.A., Young, K.M., and Perry, M.E. (2003). mdm2 Is critical for inhibition of p53 during lymphopoiesis and the response to ionizing irradiation. Mol. Cell. Biol. *23*, 462–472.

Meyer, K.D., Lin, S.C., Bernecky, C., Gao, Y., and Taatjes, D.J. (2010). p53 activates transcription by directing structural shifts in Mediator. Nat. Struct. Mol. Biol. *17*, 753–760.

Nigro, J.M., Baker, S.J., Preisinger, A.C., Jessup, J.M., Hostetter, R., Cleary, K., Bigner, S.H., Davidson, N., Baylin, S., Devilee, P., et al. (1989). Mutations in the p53 gene occur in diverse human tumour types. Nature *342*, 705–708.

Olive, K.P., Tuveson, D.A., Ruhe, Z.C., Yin, B., Willis, N.A., Bronson, R.T., Crowley, D., and Jacks, T. (2004). Mutant p53 gain of function in two mouse models of Li-Fraumeni syndrome. Cell *119*, 847–860.

Ourliac-Garnier, I., and Londoño-Vallejo, A. (2011). Telomere strand-specific length analysis by fluorescent in situ hybridization (Q-CO-FISH). Methods Mol. Biol. *735*, 33–46.

Parry, E.M., Alder, J.K., Lee, S.S., Phillips, J.A., 3rd, Loyd, J.E., Duggal, P., and Armanios, M. (2011a). Decreased dyskerin levels as a mechanism of telomere shortening in X-linked dyskeratosis congenita. J. Med. Genet. *48*, 327–333.

Parry, E.M., Alder, J.K., Qi, X., Chen, J.J., and Armanios, M. (2011b). Syndrome complex of bone marrow failure and pulmonary fibrosis predicts germline defects in telomerase. Blood *117*, 5607–5611.

Pereboom, T.C., van Weele, L.J., Bondt, A., and MacInnes, A.W. (2011). A zebrafish model of dyskeratosis congenita reveals hematopoietic stem cell formation failure resulting from ribosomal protein-mediated p53 stabilization. Blood *118*, 5458–5465.

Poyurovsky, M.V., Katz, C., Laptenko, O., Beckerman, R., Lokshin, M., Ahn, J., Byeon, I.J., Gabizon, R., Mattia, M., Zupnick, A., et al. (2010). The C terminus of p53 binds the N-terminal domain of MDM2. Nat. Struct. Mol. Biol. *17*, 982–989.

Prophet, E., Mills, B., Arrington, J., and Sobin, L. (1992). Laboratory Methods in Histotechnology (Washington, DC: AFIP).

Simeonova, I., Lejour, V., Bardot, B., Bouarich-Bourimi, R., Morin, A., Fang, M., Charbonnier, L., and Toledo, F. (2012). Fuzzy tandem repeats containing p53 response elements may define species-specific p53 target genes. PLoS Genet. *8*, e1002731.

Srivastava, S., Zou, Z.Q., Pirollo, K., Blattner, W., and Chang, E.H. (1990). Germ-line transmission of a mutated p53 gene in a cancer-prone family with Li-Fraumeni syndrome. Nature *348*, 747–749.

Tafvizi, A., Huang, F., Fersht, A.R., Mirny, L.A., and van Oijen, A.M. (2011). A single-molecule characterization of p53 search on DNA. Proc. Natl. Acad. Sci. USA *108*, 563–568.

Takenaka, I., Morin, F., Seizinger, B.R., and Kley, N. (1995). Regulation of the sequence-specific DNA binding function of p53 by protein kinase C and protein phosphatases. J. Biol. Chem. *270*, 5405–5411.

Terzian, T., Wang, Y., Van Pelt, C.S., Box, N.F., Travis, E.L., and Lozano, G. (2007). Haploinsufficiency of Mdm2 and Mdm4 in tumorigenesis and development. Mol. Cell. Biol. *27*, 5479–5485.

Toledo, F., and Wahl, G.M. (2006). Regulating the p53 pathway: in vitro hypotheses, in vivo veritas. Nat. Rev. Cancer *6*, 909–923.

Toledo, F., Krummel, K.A., Lee, C.J., Liu, C.W., Rodewald, L.W., Tang, M., and Wahl, G.M. (2006a). A mouse p53 mutant lacking the proline-rich domain rescues Mdm4 deficiency and provides insight into the Mdm2-Mdm4-p53 regulatory network. Cancer Cell *9*, 273–285.

Toledo, F., Liu, C.W., Lee, C.J., and Wahl, G.M. (2006b). RMCE-ASAP: a gene targeting method for ES and somatic cells to accelerate phenotype analyses. Nucleic Acids Res. *34*, e92.

Ventura, A., Kirsch, D.G., McLaughlin, M.E., Tuveson, D.A., Grimm, J., Lintault, L., Newman, J., Reczek, E.E., Weissleder, R., and Jacks, T. (2007). Restoration of p53 function leads to tumour regression in vivo. Nature *445*, 661–665.

Vulliamy, T.J., Kirwan, M.J., Beswick, R., Hossain, U., Baqai, C., Ratcliffe, A., Marsh, J., Walne, A., and Dokal, I. (2011). Differences in disease severity but similar telomere lengths in genetic subgroups of patients with telomerase and shelterin mutations. PLoS One *6*, e24383.

Walne, A.J., Vulliamy, T., Kirwan, M., Plagnol, V., and Dokal, I. (2013). Constitutional mutations in RTEL1 cause severe dyskeratosis congenita. Am. J. Hum. Genet. *92*, 448–453.

Wang, Y.V., Leblanc, M., Fox, N., Mao, J.H., Tinkum, K.L., Krummel, K., Engle, D., Piwnica-Worms, D., Piwnica-Worms, H., Balmain, A., et al. (2011a). Fine-tuning p53 activity through C-terminal modification significantly contributes to HSC homeostasis and mouse radiosensitivity. Genes Dev. *25*, 1426–1438.

Wang, Y., Shen, M.F., and Chang, S. (2011b). Essential roles for Pot1b in HSC self-renewal and survival. Blood *118*, 6068–6077.

Zhong, F., Savage, S.A., Shkreli, M., Giri, N., Jessop, L., Myers, T., Chen, R., Alter, B.P., and Artandi, S.E. (2011). Disruption of telomerase trafficking by TCAB1 mutation causes dyskeratosis congenita. Genes Dev. *25*, 11–16.